RSC Advances

PAPER

Check for updates

Cite this: *RSC Adv.*, 2020, **10**, 24653

Preparation of PVDF/FMBO composite electrospun nanofiber for effective arsenate removal from water

Parisa Aliahmadipoor,[a] Dadkhoda Ghazanfari,*[a] Rasoul Jamshidi Gohari*[b] and Mohammad Reza Akhgar[a]

In this study, novel electrospun nanofibers (NFs) composed of organic polyvinylidine fluoride (PVDF) and inorganic Fe–Mn binary oxide (FMBO) nanoparticles were fabricated using an electrospinning technique for adsorptive decontamination of As(v) from polluted water. The NFs were prepared with doped solutions consisting of different weight ratios of PVDF/FMBO, in a NF matrix, ranging from 0 to 0.5. SEM, XRD, FTIR and TEM then characterized the NFs and FMBO particles. The XRD analysis indicated successful impregnation of FMBO nanoparticles in the NF matrix of the NFs investigated. An As(v) adsorption capacity as high as around 21.32 mg g^{-1} was obtained using the NF containing the highest amount of FMBO nanoparticles (designated as PVDF/FMBO 0.5). Furthermore, the adsorptive performance of the PVDF/FMBO 0.5 nanofiber could be easily regenerated using diluted alkaline solution (NaOH and NaOCl).

Received 24th March 2020
Accepted 28th May 2020

DOI: 10.1039/d0ra02723e

rsc.li/rsc-advances

1. Introduction

Nowadays, the toxicity of hazardous arsenic in drinking water is well known and many organizations around the world have adjusted the maximum acceptable concentration of heavy metals in contaminated water to very low concentrations. Stringent drinking water regulations are made in order to lower the maximum contaminated level (MCL).[1–3] For instance, since 2006 the World Health Organization (WHO) have decided to reduce the maximum arsenic concentration in drinking water from 50 parts per billion (ppb) to 10 ppb.[4] The existence of arsenic in drinking water has been reported in many countries like the USA, China, Bangladesh, India and Iran.[5] Generally, human exposure to arsenic compounds comes from polluted water, food and air contaminated by industrial and agricultural activities. This is of special concern for the reason that the liquid from arsenic is odorless and colorless, making it impossible to recognize by sight only.[6,7] Some studies show that long term drinking of arsenic contaminated ground water can lead to cancer of the bladder, lungs, skin, kidney and liver. The World Health Organization (WHO) has been well known to establish standards for arsenic in drinking water since 1958.[8] Nowadays, the guideline for acceptable arsenic concentration in drinking water is 10 ppb.[1] The stiffening of regulations generates strong demands to improve methods for removing toxic heavy metals from drinking water.[3] To perform this task numerous techniques such as chemical precipitation,[9] Coagulation and flocculation,[10] biological process,[11] ion exchange technique,[12] adsorption process and membrane technologies[13,14] extensively have been used for arsenic removal. However, the major drawbacks of the removal techniques: chemical precipitation and coagulation process are commonly failure to meet the required standards, ion exchange and membrane technologies are considered as expensive methods.[15] On the other hand, adsorption process has some advantages such as easy to handle and operation, the efficiency is good but the cost is relatively low.[16,17] Apart from this the efficiency of removal is mostly dependent on the materials design. Numerous nano adsorbent materials have been used in the recent years, among them the common are ferric oxides,[18] manganese oxides,[19] titanium oxides,[20] magnesium oxides,[21] zinc oxides[22] and *etc.* Based on the open literature, a novel Fe–Mn binary oxide (FMBO) nano particle, which combines the oxidation property of manganese dioxide and the high adsorption features of iron oxides to As(v) was widely explored as highly efficient adsorbent for arsenic decontamination from water/wastewater. FMBO exhibit various advantages such as fast kinetics, high adsorption capacity, and preferable sorption toward arsenic.[23] Nevertheless, to further promote the practical application of nano sized FMBO particles in abatement of arsenic pollution, there are some technical bottlenecks to be solved. For instance, when nano sized adsorbent applied in aqueous solution they tend to aggregate into large size particles and their adsorption capacity loss seems inevitable.[24] In addition, how to efficiently and costly separate 100% of the exhausted nano sized metal oxides from water/wastewater still remains an interesting but challenging task also frequently

[a]*Department of Chemistry, Kerman Branch, Islamic Azad University, Kerman, Iran. E-mail: ghazanfari@iauk.ac.ir*

[b]*Department of Chemical Engineering, Bardsir Branch, Islamic Azad University, Bardsir, Iran. E-mail: rjgohari@bardsiriau.ac.ir*

This article is licensed under a Creative Commons Attribution-NonCommercial 3.0 Unported Licence.

associated with problems like activity loss because of agglomeration and excessive pressure drops while used in flow through process. Fortunately, fabrication of new nano sized adsorbents based composite adsorbents seems to be an effective approach to respond to all the above technical problems.[25] To promote the use of metal oxides adsorbent nanoparticles in actual purification processes, many researchers have focused on the impregnation of nanoparticles adsorbent on some host medias such as bentonite,[26] zeolite,[27] chitosan,[28] diatomite,[29] cellulose,[30] graphene oxide[31] and also porous polymers.[32] In recent decades, electrospun nanofibers due to their unique functional properties such as porous structure, large surface area and high mechanical strength have obtained much interest for use in water purification processes.[13,33] In continuation of our previous studies on fabrication nanocomposites that were composed of on organic polymer and inorganic nano sized metal oxide adsorbents for heavy metals removal.[34–36] The present study aims to synthesis new type of electrospun PVDF/FMBO composite nanofiber by electrospinning method for As(v) ions decontamination from aqueous solutions.

2. Experimental procedure

2.1. Material

All chemicals were analytical grade from Merck Chemicals Co. Polyvinylidene fluoride (PVDF, MFCD00084470) was selected as basic material for synthesize of nanofibers. Dimethylformamide (DMF) and polyvinylpyrrolidone (PVP, 5295 Millipore) were used as solvent and additive, respectively. Ferrous sulphate hepta hydrate ($FeSO_4 \cdot 7H_2O$), potassium permanganate ($KMnO_4$), sodium hydroxide (NaOH) were applied to synthesis of FMBO nanoparticles (NFs). To prepare feed solution containing specific concentration of As(v), standard solution of arsenic supplied. Sodium hypochlorite (NaClO) was used with NaOH to prepare a solution mixture to regeneration of the adsorptive efficiency of the electrospun nanofibers prepared.

2.2. Synthesis of FMBO particles

FMOB nanoparticles prepared with Fe/Mn molar ratio of 3 : 1 as described in our previous research.[34] At first, 11.85 grams of $KMnO_4$ and 62.55 grams of $FeSO_4 \cdot 7H_2O$ were dissolved separately in 100 mL deionized water. After mixing the solutions with a magnetic stirrer for 20 minutes, NaOH 3 M was added to adjusted the solution pH to around 8. The stirring of solution was continued until the precipitates to be formed. Then, the solution was filtrated and the precipitates were washed with deionized water. It was dried at 70 °C for 48 hours. At last, the synthesized FMBO nano particles was ground and stored in a lab desiccator until use.

2.3. Preparation of PVDF/FMBO electrospun nanofibres

Electrospinning is extensively used to develop nanofibers with high tensile strength, which is desirable in applications due to their unique electrical, and mechanical properties, as well as the differences in surface morphology of the solvent-cast. The ability to align and control fiber diameter makes this technique highly attractive, contribute to better dispersion of nanoparticles with the lower viscosity of the polymer solution and changing the electric field applied between the source and collector provided manifold possibilities for the nanostructure and continuous process that results in longer fibers than generated fiber compared to other similar techniques in a controllable manner as well as the differences in surface morphology and properties of nanofibers. Also, in principle, electrospinning improves removal of organic solvent after casting, which has environmental implication.[37–39] Table 1 presents the composition of dope solutions prepared for synthesizing four different types of electrospun PVDF/FMBO NFs. For electrospinning a mixture was firstly prepared by dissolving PVP as pore former agent in DMF solvent. According to the obtained results, DMF was found to be the most favorable solvent for the electrospinning process. Evidence indicating that the morphology and beads formation on the fiber structure was more correlated with the solution properties used. This is attributed to the better electrical conductivity, lower viscosity and higher dielectric properties that are known to be the most important parameters affecting fiber morphology and lead to extensive jet splashing, resulting in bead formation and reduced fiber diameter.[38,40] Predetermined amount of FMBO nanoparticle adsorbent with high adsorption capacity and selectivity for decontaminating of the hazardous arsenic anions from polluted water samples was added to DMF and stirred to 24 h until to give homogenous solution with well-dispersed nanoparticles. In order to increase system productivity, fabricated nanofibers must have high permeability, good hydraulic properties and excellent chemical resistance. Among the polymer materials available, in the case of polymer matrix, PVDF as a semi-crystalline fluoropolymer is one of the most used membrane materials. It is synthesized by the free radical polymerization of 1,1-difluoroethylene ($CH_2{=}CF_2$) and usually contain 59.4% fluorine and 3% hydrogen and due to high polarizability of the CH_2 and CF_2 groups on the polymer chain, it is an electroactive thermoplastic polymer. It is also one of the most widely used numerous technological applications

Table 1 Composition of FMBO/PVDF dope solution

Nanofibers	FMBO/PVD ratio	PVDF (wt%)	PVP (wt%)	DMF (wt%)	FMBO (wt%)
N 0 (control)	0.0	15.00	1.50	83.50	—
N 0.125	0.125	14.72	1.47	81.96	1.84
N 0.25	0.25	14.45	1.44	80.48	3.61
N 0.5	0.5	13.95	1.40	77.67	6.98

 This journal is © The Royal Society of Chemistry 2020

materials as well as the constituent superior properties of nanofibers, and high tensile strength pressure resistance.[41,42] Outstanding nanofiber forming ability, and chemical resistance to wide range of pH, has been selected as nanofiber material in this study. Then pre-weighed amount of dried PVDF pellets was gradually added to the solution that was under continuous stirring at a temperature of 80 °C. In order to remove the microbubbles dissolved in the suspension it was sonicated for 180 min. PVDF–FMBO nanofibers were synthesis with the homogeneous dope solutions in ratio from 0.125–0.5 by electrospinning technique. Specifically, experiments were performed with a thin nozzle with an internal diameter of about 100 μm with fixed tip to collector distance of 17 cm and applied voltage 17.5 kV. All nanofibers were dried at room temperature.

2.4. Batch As(v) adsorption study

The adsorption behavior of As(v) by prepared nanofibers was investigated with the batch experiments. As(v) solutions with initial concentration ranging from 10 to 70 mg L^{-1} were prepared by dissolving predetermined amount of standard arsenic solution in deionized water. All adsorption isotherm experiments were performed in Erlenmeyer flasks with 200 mL

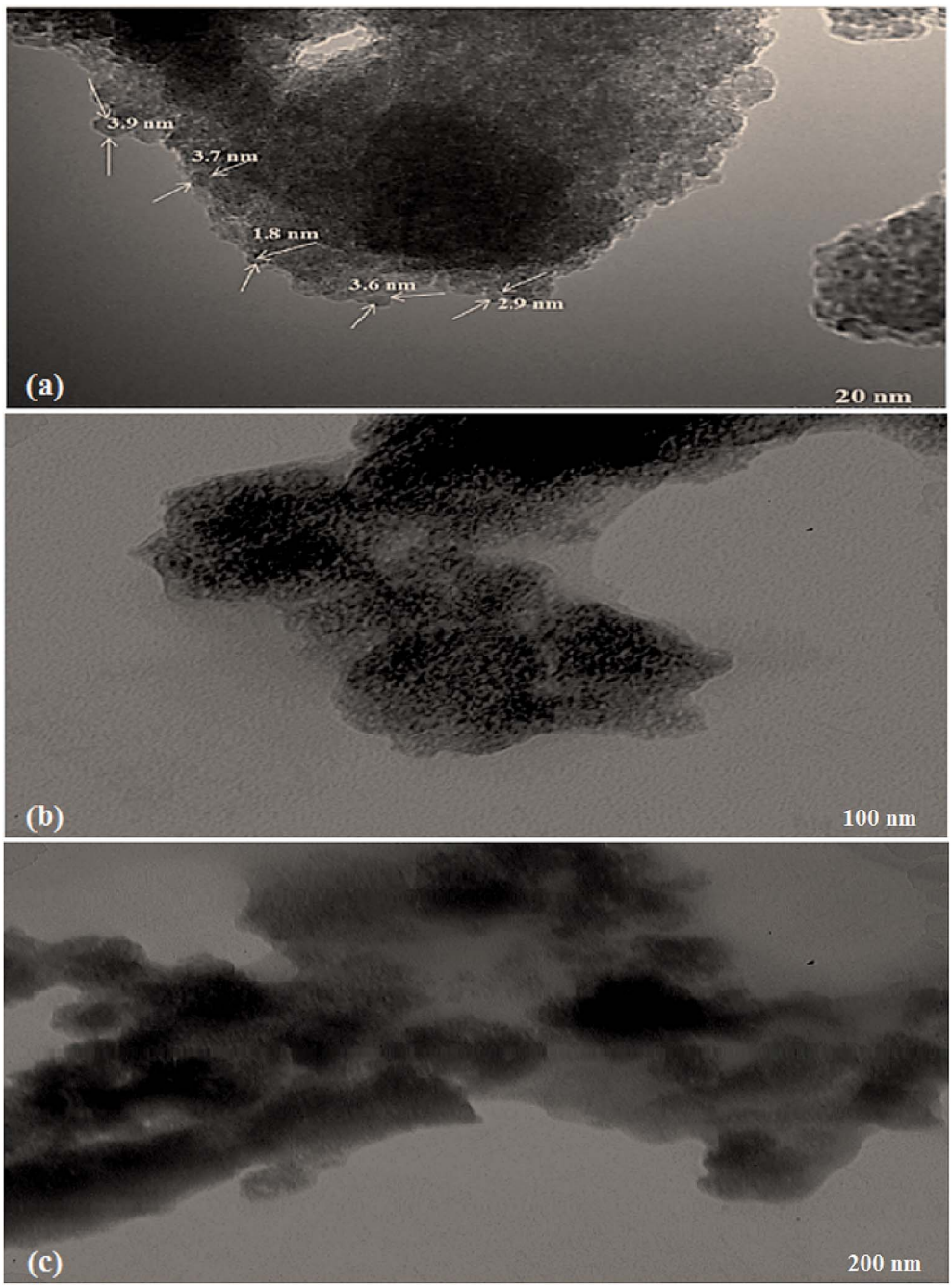

Fig. 1 The morphologies of the synthesized FMBO nanoparticles at different magnification ranges (a) 20 nm (b) 100 nm (c) 200 nm.

of As(v) solutions and containing 0.2 g of nanofiber (which was cut in small pieces), and pH of the solution was adjusted using HCl or NaOH solution. The flasks were continuously shaken by using a rotary shaker with a speed of 180 rpm for 48 hours at room temperature. The concentrations of residual As(v) were analyzed by using flame atomic absorption spectrometer (FAAS, Varian, Spectra A 220). All samples were measured twice and the average was recorded.

The equilibrium adsorption amount and removal efficiency of As(v) by the nanofibers were calculated as follows:

$$q_e = \frac{(C_0 - C_e)V}{M_m} \quad (1)$$

where q_e is the equilibrium adsorbed amount of As(v) per nanofiber weight (mg g^{-1}), C_0 and C_e are initial (mg L^{-1}) and equilibrium concentrations (mg L^{-1}) of As(v) in the solution, respectively, V is the volume (L) of the As(v) solution and M_m is the mass (g) of dry nanofiber used in the experiments.

2.5. pH effect study

The effect of pH on As(v) adsorption was studied by adding the same weight of the nanofibers with the maximum adsorption capacity in the 100 mL of the 30 mg L^{-1} As(v) solution at different pH ranging between 4–12. The pH of As(v) solution was adjusted using either 0.1 M NaOH or HCl aqueous solution. After shaking for 48 h at 25 °C, the concentration of As(v) of each pH solution was determined by FAAS. After evaluating the nanofiber's adsorption capacities, the optimum pH was determined.

2.6. Characterizations

X-ray diffraction (XRD) study of the synthesized FMBO particles and nanofibers were recorded by an X-ray diffractometer (Model D8 Advance, Bruker). FTIR spectra of the synthesized FMBO nanoparticles before and after As(v) adsorption process were obtained at room temperature using FTIR spectroscopy (Model Tensor 27, Bruker) in the wave number range of 400–2400 cm^{-1}. A scanning electron microscope (SEM) (TM 3000, Hitachi, Japan) was used to observe the top surface of the PVDF/FMBO NFs. The morphology of the FMBO sample synthesized in this work were characterized using a transmission electron microscope (TEM) (HT 7700, Hitachi).

3. Results and discussion

3.1. Characterization of the FMBO nanoparticles and nanofibers

In order to obtain more information about the morphologies of nanoparticles, FMBO was characterized by TEM, XRD and FTIR.

TEM images have been taken at different magnification ranges (20, 100 and 200) to visualize the size and surface morphology of FMBO nanoparticles (Fig. 1). Fig. 1(a) represents that the average particle size of the FMBO nanoparticles are less than 4 nm. In addition, the presence of amorphous structure of the FMBO nanoparticles can be observed from both the low and high magnification of TEM images (Fig. 1(a) and (c)). The aggregation of regular nanosized FMBO particles might be ascribed to the amorphous structure and nature of FMBO particles, which is consistent with the TEM images of FMBO particles in the studies of Yang *et al.* (2019) and Ye *et al.* (2015).[43,44]

The XRD pattern of the FMBO nanoparticles, the PVDF and the PVDF/FMBO nanofiber are presented in Fig. 2. The XRD FMBO particles, shows an obvious peak at 2θ of 34.5°, indicating that the Fe–Mn binary oxide exists only in amorphous form, which was in agreement with the characteristic of FMBO reported by the Zhang *et al.* in 2007.[23]

The PVDF nanofiber in 2θ showed a broad peak at 15–23 and a strong peak at 29–30, which can be attributed to its semi-crystalline structure polymer that also reported by Yoon and Kelarakis in 2014.[45] The presence of an obvious peak at 2θ of 34.5° in the PVDF/FMBO-0.5 nanofibers reveal the effective impregnation of FMBO particles on the PVDF NFs.

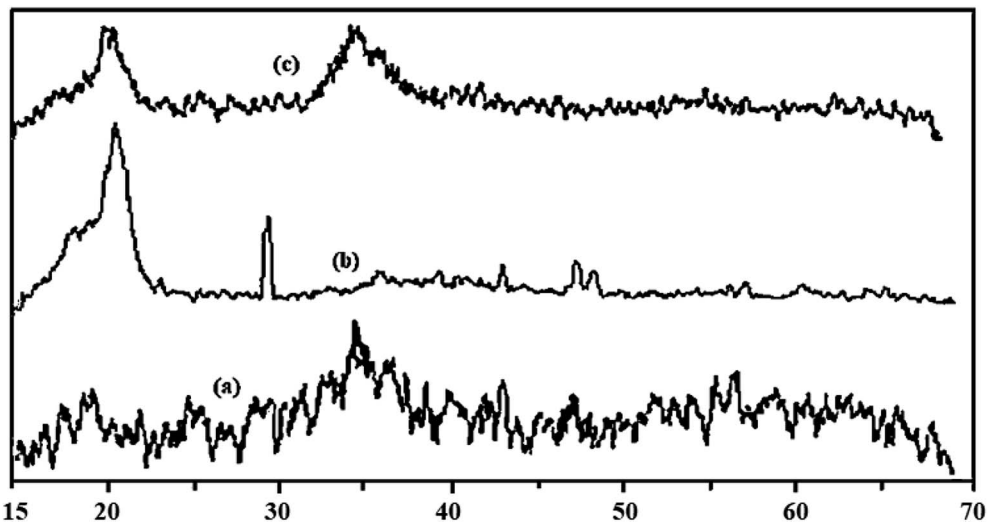

Fig. 2 XRD patterns of (a) FMBO particles, (b) PVDF nanofiber and (c) FMBO/PVDF nanofiber.

 This journal is © The Royal Society of Chemistry 2020

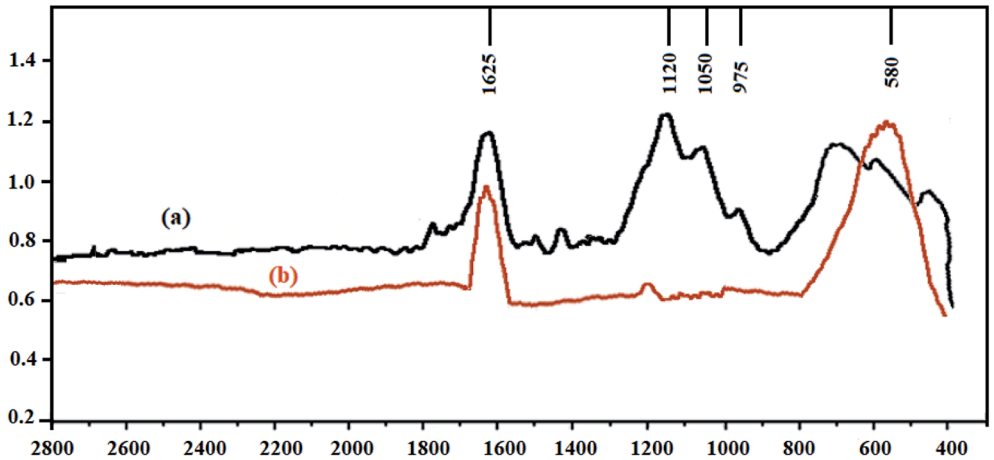

Fig. 3 FTIR spectrum of FMBO particles before (a) and after (b) arsenate adsorption experiments.

Fig. 3 shows the FTIR (ATR, Bruker, Tensor 27) spectra of FMBO particles before and after As(v) adsorption by immersing the particles in a solution containing 50 ppm As(v). A peak appeared at 1625, before the As(v) uptake that could be assigned to deforming water molecules indicating the presence of physisorbed water on the oxides. Three peaks at 1120, 1050, and 975 were related to Fe–O and aqua-complex of Fe–OH, respectively. When As(v) was adsorbed, the latter three peaks were practically disappeared and a new peak was observed at 580 which can be explained by the presence of As–O–Fe vibration in

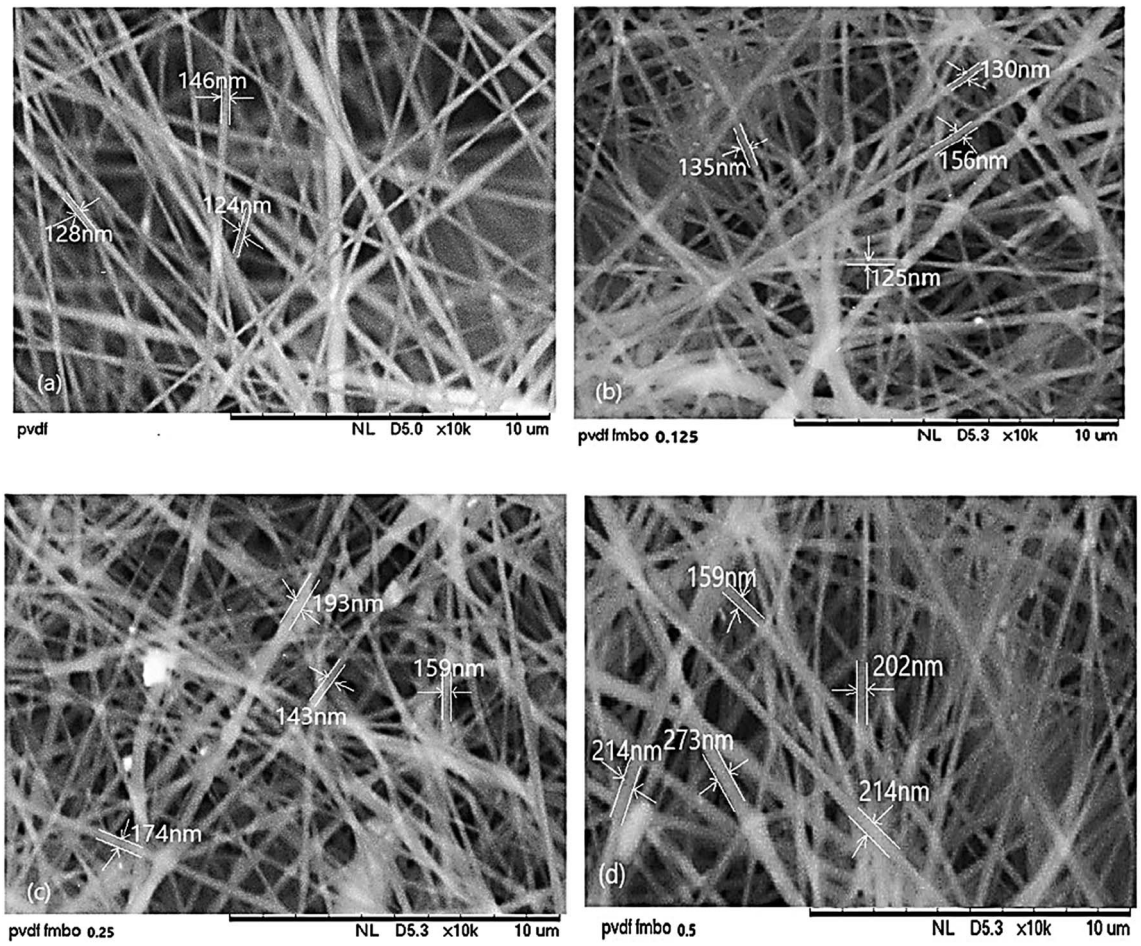

Fig. 4 SEM micrographs of top surface of nanofibers prepared with different FMBO/PVDF weight ratios, (a) PVDF, (b) FMBO/PVDF-0.125, (c) FMBO/PVDF-0.25, (d) FMBO/PVDF-0.5.

Table 2 Nanofibers orientation and coherency

Samples	Orientation (°)	Coherency
PVDF	−17.5	0.086
PVDF/FMBO 0.125	−10.45	0.084
PVDF/FMBO 0.25	−9.3	0.073
PVDF/FMBO 0.5	−1.56	0.01

the adsorbed As(v) ions which is consistent with FTIR patterns of Liang *et al.* (2020).[46]

Fig. 4 shows the top surface SEM micrographs of all fabricated NFs at this study. These figures represent the formation of ultrafine fibers having diameter in the range of 124–273 nm. Generally, it has been found that tip-to-collector distance has an influence on the structural morphology and average nanofiber's diameter. The effect of the distance between the needle and the ground collector on the mean fiber diameter was also investigated. The selected tip-to-collector distances were 14, 17 and 20 cm. By varying this parameter, we could determine the optimum distance was 17 cm, which was long enough for stretching and solvent evaporation. A similar structure and clear difference was also observed under constant voltage conditions, as the distance increased from 14 to 20 cm, there was no significant effect on the morphology of the fabricated electrospun nanofibers at various distances. While, the average fiber diameter showed a decreasing trend and with increasing distance, the mean fiber diameter decreased, which was consistent with the results by researchers Zulfikar *et al.* (2018) and Motamedi *et al.* (2017). It was also found that the size of the fibers changes by increasing the loading of FMBO nanoparticles.[41,47] The nanofibers orientation was determined by measuring SEM images coherency with Image J software (Image J 1.44p). The coherency indicates if the local image features are oriented or not: it is 1 for ideal local orientation and it is 0 for isotropic gray value structures. From results Table 2, it was found that the NFs containing the highest amount of FMBO nanoparticles (PVDF/FMBO 0.5) had higher orientation than the other fabricated nanofibers.

The XRD pattern of Fe–Mn binary adsorbent also showed that no obvious crystalline peak was detected, indicating that both the Fe oxide and Mn oxide of the Fe–Mn binary composite exist mainly in amorphous form, which may be responsible for the high surface area that is according of Zhang reported in 2007.[23]

3.2. Adsorption study on the PVDF/FMBO NFs

3.2.1. Effect of pH. PVDF/FMBO-0.5 was selected for the evaluation of pH effect on As(v) adsorption, in order to the highest As(v) adsorption rate among the nanofibers prepared. Fig. 5 indicates the efficiency of As(v) removal along with pH changes between 4 to 12. Obviously, as the figure shows, As(v) elimination was closely associated with pH changes, indicating that the highest adsorption could occur in acid context, while increased pH led to its reduction. This effect is due to the strongly competition of hydrogen ions with arsenate ions to occupy the adsorption sites. Elimination of As(v) had its optimal conditions over pH 4 regarding PVDF/FMBO-0.5 nanofibers. $H_2AsO_4^-$ and $HAsO_4^{2-}$ are predominant As(v) types in the solution under the experimental pH range of 3 to 11. Lower pH will be ideal to protonate sorbent surface and at low pH value,[4] the impregnated FMBOs on the surface of nanofibers would be protonated. It is assumed that higher protonation enhances the locations with positive charge.[48] As a result, there will be an attraction force between the sorbent surface and As anions which will increase the amount of adsorption in the lower pH region. In the sites with higher pH, the repulsion effect would increase, which leads to sharp decrease in arsenate adsorption in the pH > 10. Clearly, PVDF/FMBO-0.5 had the potential to result in at least 30% As(v) elimination at a pH range of 4–8 after 48 hours' contact, primary As(v) concentration for testing was 30 mg L^{-1}. Since the ground water has a pH range of 6–8, the

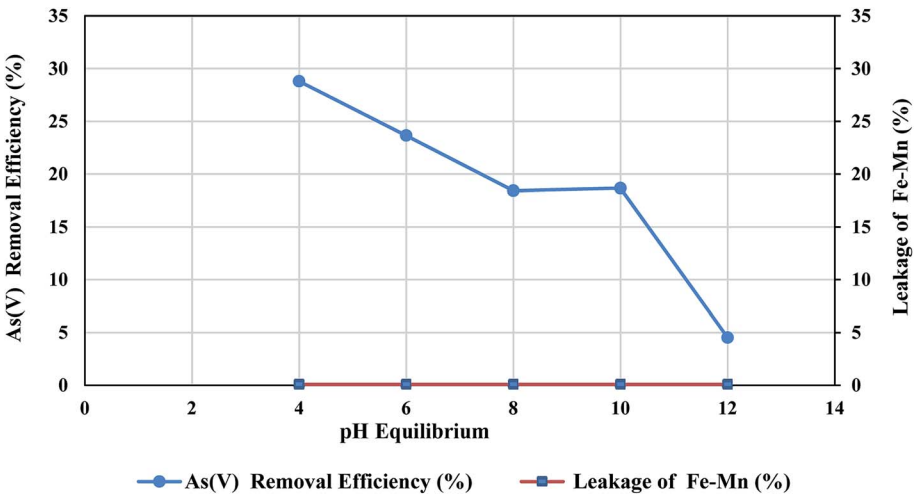

Fig. 5 Effect of initial pH on As(v) removal by PVDF/FMBO-0.5 (operating conditions: initial concentration of As(v) = 30 mg L^{-1}, nanofibers weight = 0.2 g L, stirring speed = 200 rpm, temperature = 25 °C and contact time = 48 h).

 This journal is © The Royal Society of Chemistry 2020

studied nanofibers are good candidates to be applied in water treatment with no adjusted pH.

According to the Fig. 5 FMBO leakage from the nanofiber was negligible at the studied pH ranges, which confirms that FMBO has completely impregnated in nanofibers and would lead to no hazardous effects for human health.

3.2.2. Adsorption isotherm. The FMBO nanoparticles incorporated in PVDF nanofibers have novel nano-size and amorphous structure. In addition, they have been used due to their many active surface sites for arsenic adsorption from contaminated water samples. First As(v) separates from the surface of the solution and causes the formation of abandoned arsenic ions inside the aqueous solution. Then during the process, new active adsorbent sites are formed on the surface of impregnated FMBO nanoparticles in the nanofibers. The new active sites adsorb arsenate ions on the FMBO nano particles by forming a surface complex. This process continues until As(v) ions and active surface sites are available. When FMBO particles adsorb a significant amount of As(v), the rate of arsenate adsorption decreases. This process continues until the nanocomposite As(v) adsorption capacity stops.[49,50] The isotherm experiments were conducted to evaluate adsorption capacities of the PVDF NFs in the absence and presence of FMBO adsorbent showed in Fig. 6. The adsorption potential of the N0 nanofiber was not considered here due to it has no capacity of adsorbing As(v) because the FMBOs were absent in the nanofibers matrix. According to the results, the highest As(v) adsorption capacities that could be achieved by NF-0.125, NF-0.25 and NF-0.5 nanofibers were 13.77, 17.69 and 21.32 mg g^{-1}, respectively. With increasing FMBO/PVDF proportion from 0.125 to 0.5, led to significant improvement of the adsorption capacity of NF, which could be associated with the presence of a larger quantity of adsorbent available to adsorb higher As(v) ratios.

A comparison table has been made for different adsorbents. It has been reported that the maximum As(v) adsorption capacity of different adsorbents which is listed in Table 3.

There are two different famous models including Langmuir and Freundlich, that may describe the As(v) adsorption process. The Langmuir model can be written as:

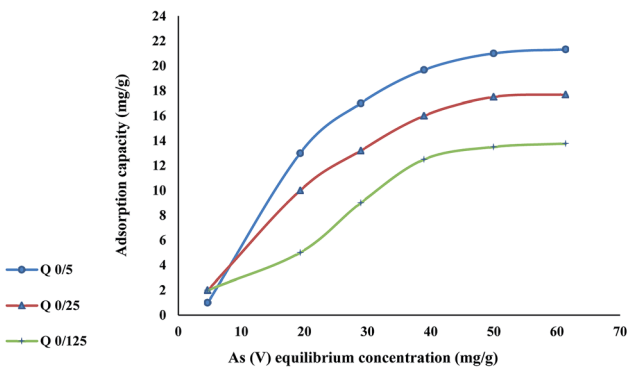

Fig. 6 Adsorption isotherms for As(v) by NFs with different FMBO/PVDF ratio (a) NF-0.125, (b) NF-0.25 and (c) NF-0.5 nanofibers (experimental conditions: nanofiber weight = 0.2 g, temperature = 25 °C, contact time=24 h).

Table 3 Comparison of maximum As(v) adsorption capacities for different adsorbents

Adsorbent	pH	As(v) adsorption capacity (mg g^{-1})	Reference
Iron-oxide-coated manganese sand	7.0	5.452	51
Surface-modified diatomite	7.0	8.0	52
PVDF/FMBO NFs	7.0	21.32	This study
Iron-modified activated carbon	7.6–8.0	51.3	53
Iron oxide coated sponge	6.5–7.3	4.6	54
PVDF/zirconium membrane	3–4	21.5	55
Iron-impregnated tablet ceramic	6.9	8.49	56
Iron hydro(oxide) nanoparticles on to activated carbon	7.0	4.56	57
Nano sized iron oxide-coated perlite	4–8	0.39	58
Nano-iron–titanium mixed oxide	7.0	14.0	59
Surface-modified diatomite	7.0	8.0	60

$$q_e = \frac{q_m b c_e}{1 + b c_e} \quad (2)$$

where q_e is the amount of As(v) adsorbed onto the PVDF/FMBO nanofibers (mg g^{-1}), C_e is equilibrium concentration of the As(v) in the solution phase (mg L^{-1}), q_m is the maximum amount of adsorbed As(v) per unit weight of PVDF/FMBO nanofibers (mg g^{-1}) and b is the Langmuir reaction constant (L mg^{-1}) related to free energy of adsorption.

The Freundlich isotherm model is often expressed.

$$q_e = K_f c_e^{1/n} \quad (3)$$

where q_e and C_e are previously defined, K_f is a constant concerned with adsorption capacity of the nanofiber adsorbents (mg g^{-1}) and n is the heterogeneity factor which is concerned with the adsorption intensity.

Table 4 shows the Langmuir and Freundlich isotherm factors for As(v) uptake on adsorptive nanofibers at pH 4, higher coefficients R^2 value suggested that Langmuir model was suitable for describing the adsorption behavior of As(v) by nanofibers.

3.2.3. Adsorption kinetics. The kinetic experiments were performed to determine the effect of the contact time as an important factor along with the rate of As(v) elimination using the adsorbent. Fig. 7 shows the influence of time on the kinetics of As(v) removal using NF the PVDF/FMBO-0.5 having significant adsorption potential at specific intervals from 0 to 20 h. The primary concentrations of As(v) solution considered to 20 ppm. The result shows changes in the As(v) concentration with increasing contact time, until the adsorption capacity of

Table 4 Langmuir and Freundlich isotherm parameters for As(v) adsorption on nanofibers

	Langmuir model			Freundlich model		
Nanofibers	q_m (mg g^{-1})	b (L mg^{-1})	R^2	K_f (mg g^{-1})	n	R^2
N 0.125	13.77	0.04	0.9963	1.39	1.9673	0.9682
N 0.25	17.69	0.064	0.9964	2.25	2.1281	0.9707
N 0.5	21.32	0.066	0.9999	2.69	1.0253	0.9756

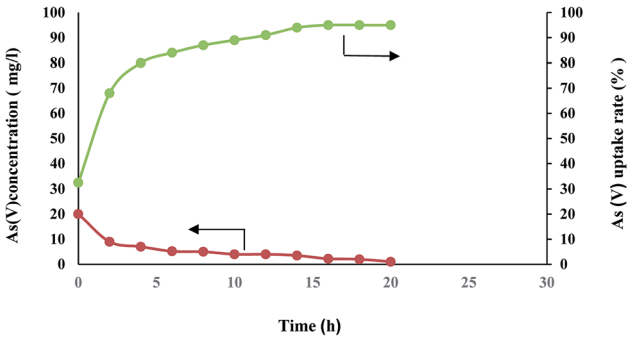

Fig. 7 Variation of As(v) adsorption kinetics onto the PVDF/FMBO-0.5 nanofibers with time (operating conditions: initial As(v) concentration (C_0) = 20 mg L^{-1}, temperature = 25 °C, nanofiber weight = 0.2 g and equilibrium time = 10 h).

NFs can be stopped. The first 4 hours experience a high initial removal was observed that indicating an 80% uptake of the initial As(v) amount. This can be due to the small dimensions of FMBO particles, which would be provide the high availability of adsorption sites at the start of adsorption. It is may be that the adsorption capacity is proportional to the number of active sites on the surface of the FMBO.

3.3. Performance of NFs in As(v) removal after regeneration process

In order to evaluate the reusability of the arsenate saturated NFs-0.5 adsorbent, the regeneration tests were then carried out using an alkaline solution containing of diluted NaOH and NaOCl. After regeneration process, experimented results indicated that nearly 70% of the adsorption potential of NFs-0.5 could be regenerated.

4. Conclusion

Electrospun PVDF nanofibers were successfully fabricated by embedding inorganic FMBO adsorbent to develop a novel, efficient and environmental friendly technology with low cost and low energy consumption for arsenate decontamination from contaminated drinking water. The XRD study showed effective impregnation of FMBO nanoparticles on the PVDF NFs. The FTIR studies revolved successful As(v) adsorption by FMBO nanoparticles.

The SEM micrographs of all fabricated NFs represented the formation of ultrafine fibers having diameter in the range of 124–273 nm. The best performing nanofiber prepared from the PVDF/FMBO ratio of 0.5 showed that maximum As(v) uptake capacity around 21.32 mg g^{-1} and this adsorption capacity is comparable to the most of the promising composite adsorbents reported in literature. Additionally, as high as 70% of the original adsorptive performance of PVDF/FMBO 0.5 nanofiber was able to be regenerated using diluted alkaline solution.

Conflicts of interest

There are no conflicts to declare.

References

1 S. Shankar, U. Shanker and S. Shikha, Arsenic contamination of groundwater: a review of sources, prevalence, health risks, and strategies for mitigation, *Sci. World J.*, 2014, **2014**, 1–18.
2 M. Lahkar and K. G. Bhattacharyya, Heavy metal contamination of groundwater in Guwahati city, Assam, India, *Int. Res. J. Eng. Technol.*, 2019, **6**(6), 1520–1525.
3 S. K. M. Gunatilake, Methods of removing heavy metals from industrial wastewater, *J. Multidiscip. Eng. Sci. Stud.*, 2015, **1**(1), 12–18.
4 S. Chen and S. W. Leung, In situ arsenic removal in groundwater for rural communities by iron sorption and arsenic immobilization, *Int. Proc. Chem., Biol. Environ. Eng.*, 2016, **94**(23), 149–159.
5 M. A. Sanjrani, B. Zhou, H. Zhao, S. A. Bhutto, A. S. Muneer and S. B. Xia, Arsenic contaminated groundwater in China and its treatment options, *Appl. Ecol. Environ. Res.*, 2019, **17**(2), 1655–1683.
6 J. Arif Tasleem, A. Mudsser, S. Kehkashan, A. Arif, C. Inho, M. Qazi and H. Rizwanul, Heavy metals and human health: mechanistic insight into toxicity and counter defense system of antioxidants, *Int. J. Mol. Sci.*, 2015, **16**(12), 29592–29630.
7 S. C. Santra, A. C. Samal, P. Bhattacharya, S. Banerjee, A. Biswas and J. Majumdar., Arsenic in food chain and community health risk: a study in Gangetic West Bengal, *Procedia Environ. Sci.*, 2013, **18**, 2–13.
8 E. Shokri and R. Yegani, Novel adsorptive mixed matrix membrane by incorporating modified nanoclay with amino acid for removal of arsenic from water, *J. Water Environ. Nanotechnol.*, 2017, **2**(2), 88–95.
9 M. Brbooti, B. A. Abid and N. M. Al-Shuwaiki, Removal of heavy metals using chemicals precipitation article, *J. Eng. Technol.*, 2011, **29**(3), 595–612.

 This journal is © The Royal Society of Chemistry 2020

10 X. Tang, H. Zheng, H. Teng, Y. Sun, J. Guo and W. Xie, Chemical coagulation process for the removal of heavy metals from water: a review, *Desalination Water Treat.*, 2015, **57**(4), 1733–1748.
11 I. A. Katsoyiannis and A. Zouboulis, Application of biological processes for the removal of arsenic from groundwater, *Water Res.*, 2004, **38**(1), 17–26.
12 T. Borklu Budak, Removal of heavy metals from wastewater using synthetic ion exchange resin, *Asian J. Chem.*, 2013, **25**(8), 4207–4210.
13 K. C. Khulbe and T. Matsuura, Removal of heavy metals and pollutants by membrane adsorption techniques, *Appl. Water Sci.*, 2018, **8**(19), 1–30.
14 D. Lakherwa, Adsorption of heavy metals: a review, *J. Environ. Res. Develop.*, 2014, **4**(1), 2249–3131.
15 T. Marino and A. Figoli, Arsenic removal by liquid membranes, *Membranes*, 2015, **5**, 150–167.
16 S. De Gisi, G. Lofrano, M. Grassi and M. Notarnicola, Characteristics and adsorption capacities of low-cost sorbents for wastewater treatment: a review, *Sustainable Mater. Technol.*, 2016, **9**, 10–40.
17 M. Parmar and L. Singh Thakur, Heavy Metal Cu, Ni and Zn: toxicity, health hazards and their removal techniques by low cost adsorbents: a short overview, *Int. J. Plant, Anim. Environ. Sci.*, 2013, **3**(3), 143–157.
18 D. Xu, X. Tan, C. Chen and X. Wang, Removal of Pb(II) from aqueous solution by oxidized multi walled carbon nanotubes, *J. Hazard. Mater.*, 2008, **154**, 407–416.
19 L. Feng, M. Cao, X. Ma, Y. Zhu and C. Hu, Superparamagnetic high-surface-area Fe_3O_4 nanoparticles as adsorbents for arsenic removal, *J. Hazard. Mater.*, 2012, **217**, 439–446.
20 C. Gao, W. Zhang, H. Li, L. Lang and Z. Xu, Controllable fabrication of mesoporous MgO with various morphologies and their absorption performance for toxic pollutants in water, *Cryst. Growth Des.*, 2008, **8**, 3785–3790.
21 V. K. Gupta, S. Agarwal and T. A. Saleh, Synthesis and characterization of alumina-coated carbon nanotubes and their application for lead removal, *J. Hazard. Mater.*, 2011, **185**, 17–23.
22 M. Tuzen and M. Soylak, Multi walled carbon nanotubes for speciation of chromium in environmental samples, *J. Hazard. Mater.*, 2007, **147**, 219–225.
23 G. Zhang, J. Qu, H. Liu, R. Liu and R. Wu, Preparation and evaluation of a novel Fe–Mn binary oxide adsorbent for effective arsenite removal, *Water Res.*, 2007, **41**(9), 1921–1928.
24 N. R. Nicomel, K. Leus, K. Folens, P. Van Der Voort and G. Du Laing, Technologies for arsenic removal from water: current status and future perspectives, *Int. J. Environ. Res. Public Health*, 2015, **13**(62), 1–24.
25 J. Yang, B. Hou, J. Wang, B. Tian, J. Bi, N. Wang, X. Li and X. Huang, Review nanomaterials for the removal of heavy metals from wastewater, *Nanomaterials*, 2019, **9**(3), 424.
26 M. V. Miljkovic, M. Momcilovic, M. Stankovic, B. Cirkovic, D. Laketic, G. Nikolic and M. Vujovic, Remediation of arsenic contaminated water by a novel carboxymethyl cellulose bentonite, *Appl. Ecol. Environ. Res.*, 2018, **17**(1), 733–744.
27 S. Kong, Y. Wang, Q. Hu and A. K. Olusegun, Magnetic nanoscale Fe-Mn binary oxides Loaded zeolite for arsenic removal from synthetic groundwater, *Colloids Surf., A*, 2014, **457**, 220–227.
28 S. M. Miller and J. B. Zimmerman, Novel, bio-based, photoactive arsenic sorbent: TiO_2 impregnated chitosan bead, *Water Res.*, 2010, **44**, 5722–5729.
29 M. Jang, S. H. Min, J. K. Park and E. J. Tlachac, Hydrous ferric oxide incorporated diatomite for remediation of arsenic contaminated groundwater, *Environ. Sci. Technol.*, 2007, **41**, 3322–3328.
30 X. Guo and F. Chen, Removal of arsenic by bead cellulose loaded with iron oxyhydroxide from groundwater, *Environ. Sci. Technol.*, 2005, **39**(17), 6808–6818.
31 V. Chandra, J. Park, Y. Chun, J. W. Lee, I. C. Hwang and K. S. Kim, Water-dispersible magnetite-reduced graphene oxide composites for arsenic removal, *ACS Nano*, 2010, **4**(7), 3979–3986.
32 K. Jasiewicz and R. Pietrzak, Metals ions removal by polymer membranes of different porosity, *Sci. World J.*, 2013, **2013**, 1–7.
33 V. Kumar Gupta, I. Tyagi, H. R. Sadegh, R. Shahryari Ghoshekandi, A. S. Hamdy Makhlouf and B. Maazineja, Nanoparticles as adsorbent; a positive approach for removal of noxious metal ions: a review, *Sci. Technol. Dev.*, 2015, **34**(3), 195–214.
34 R. Jamshidi Gohari, W. J. Lau, T. Matsuura and A. F. Ismail, Fabrication and characterization of novel PES/Fe–Mn binary oxide UF mixed matrix membrane for adsorptive removal of As(III) from contaminated water solution, *Sep. Purif. Technol.*, 2013, **118**, 64–72.
35 R. Jamshidi Gohari, W. J. Lau, E. Halakoo, A. Fauzi Ismail, F. Korminouri, T. Matsuura, M. S. Jamshidi Gohari and M. N. Kabir Chowdhury, Arsenate removal from contaminated water by a highly adsorptive nanocomposite ultrafiltration membrane, *New J. Chem.*, 2015, **1**(58), 1–29.
36 R. Jamshidi Gohari, W. J. Lau, T. Matsuura, E. Halakoo and A. F. Ismail, Adsorptive removal of PB(II) from aqueous solution by novel PES/HMO ultrafiltration mixed matrix membrane, *Sep. Purif. Technol.*, 2013, **120**, 59–68.
37 Z. Abu Alhasssan, Y. S. Burezq, R. Nair and N. Shehata, Polyvinylidene difluoride piezoelectric electrospun nanofibers: review in synthesis, fabrication, characterizations, and applications, *J. Nanomater.*, 2018, **2018**, 1–12.
38 B. Rezaei, A. Mousavi Shoushtari, M. Rabiee, L. Uzun, A. P. F. Turner and W. Cheung Mak, Multifactorial modeling and optimization of solution and electrospinning parameters to generate superfine polystyrene nanofibers, *Adv. Polym. Technol.*, 2018, **37**, 2743–2755.
39 K. Ghosal, A. Chandra, G. Praveen, S. Snigdha, S. Roy, C. Agatemor, S. Thomas and I. Provaznik, Electrospinning over solvent casting: tuning of mechanical properties of membranes, *Sci. Rep.*, 2018, **8**, 1–9.

40 A. Cay, E. Perrin Akçakoca Kumbasar and C. Akduman, Effects of solvent mixtures on the morphology of electrospun thermoplastic polyurethane nanofibers, *Tekst. Konfeksiyon*, 2015, **25**(1), 38–46.
41 M. A. Zulfikar, I. Afrianingsih, M. Nasir and A. Alni, Effect of Processing Parameters on the morphology of PVDF electrospun nanofiber, *J. Phys.: Conf. Ser.*, 2018, **987**, 012011.
42 V. F. Cardoso, D. M. Correia, C. Ribeiro, M. M. Fernandes and S. Lanceros-Méndez, Fluorinated polymers as smart materials for advanced biomedical applications, *Polymers*, 2018, **10**(2), 161.
43 K. Yang, Y. Liu, Y. Li, Z. Cao, C. Zhou, Z. Wang, X. Zhou, S. Ali Baig and X. Xu, Applications and characteristics of Fe-Mn binary oxides for Sb(V) removal in textile wastewater: selective adsorption and the fixed-bed column study, *Chemosphere*, 2019, **232**, 254–263.
44 S. Ye, W. Jin, Q. Huang, Y. Hu, B. Ramin Shah, S. Liu, Y. Li and B. Li, Fabrication and characterization of KGM–based FMBO–containing aerogels for removal of arsenite in aqueous solution, *RSC Adv.*, 2015, **7**, 28–57.
45 K. Yoon and A. Kelarakis, Nanoclay-directed structure and morphology in PVDF electrospun membranes, *J. Nanomater.*, 2014, **2014**, 1–7.
46 M. Liang, S. Xu, Y. Zhu, X. Chen, Z. Deng, L. Yan and H. He, Preparation and characterization of Fe-Mn binary oxide/mulberry stem biochar composite adsorbent and adsorption of Cr(VI) from aqueous solution, *Int. J. Environ. Res. Publ. Health*, 2020, **17**, 676.
47 A. Sadat Motamedi, H. Mirzadeh, F. Hajiesmaeilbaigi, S. Bagheri-Khoulenjani and M. A. Shokrgozar, Effect of electrospinning parameters on morphological properties of PVDF nanofibrous scaffolds, *Prog. Biomater.*, 2017, **6**, 113–123.
48 L. Li Min, L. Bin Zhong, Y. Ming Zheng, Q. Liu, Z. Huan Yuan and L. Ming Yang, Functionalized chitosan electrospun nanofiber for effective removal of trace arsenate from water, *Sci. Rep.*, 2016, **6**, 32480.
49 J. Nikic, M. Watson, A. Tubic, M. K. Isakovski, S. Maletic, E. Mohora and J. Agbaba, Arsenic removal from water using a one-pot synthesized low-cost mesoporous Fe–Mn-modified biosorbent, *J. Serb. Chem. Soc.*, 2019, **84**(3), 327–342.
50 G. Zhang, H. Liu, R. Liu and J. Qu, Adsorption behavior and mechanism of arsenate at Fe–Mn binary oxide/water interface, *J. Hazard. Mater.*, 2009, **168**, 820–825.
51 K. Wu, R. Liu, H. Liu, X. Zhao and J. Qu, Arsenic(III,V) adsorption on iron-oxide coated manganese sand and quartz sand: comparison of different carriers and adsorption capacities, *Environ. Eng. Sci.*, 2011, **28**, 643–651.
52 C. C. Wu, Y. C. Wang, T. F. Lin, H. L. Tsao and P. C. Chen, Removal of arsenic from waste water using surface modified diatomite, *J. Chin. Inst. Environ. Eng.*, 2005, **15**, 255–261.
53 W. Chen, R. Parette, J. Zou, F. Cannon and B. Dempsey, Arsenic removal by iron-modified activated carbon, *Water Res.*, 2007, **41**, 1851–1858.
54 T. V. Nguyen, S. Vigneswaran, H. H. Ngo and J. Kandasamy, Arsenic removal by iron oxide coated sponge: experimental performance and mathematical models, *J. Hazard. Mater.*, 2010, **182**(1–3), 723–729.
55 Y. M. Zheng, S. W. Zou, K. G. Nadeeshani Nanayakkara, T. Matsuura and J. Paul Chena, Adsorptive removal of arsenic from aqueous solution by a PVDF/zirconia blend flat sheet membrane, *J. Membr. Sci.*, 2011, **374**, 1–11.
56 R. Chen, Z. Zhang, Z. Lei and N. Sugiura, Preparation of iron-impregnated tablet ceramic adsorbent for arsenate removal from aqueous solutions, *Desalination*, 2012, **286**, 56–62.
57 C. Nieto-Delgado and J. R. Rangel-Mendez, Anchorage of iron hydro(oxide) nanoparticles onto activated carbon to remove As(V) from water, *Water Res.*, 2012, **46**, 2973–2982.
58 M. G. Mostafa, J. S. Jean, C. C. Liu, Y. C. Lee and Y. H. Chen, Kinetics and mechanism of arsenate removal by nanosized iron oxide-coated perlite, *J. Hazard. Mater.*, 2011, **187**(1–3), 89–95.
59 K. Gupta and U. C. Ghosh, Arsenic removal using hydrous nanostructure iron(III)–titanium(IV) binary mixed oxide from aqueous solution, *J. Hazard. Mater.*, 2009, **161**, 884–892.
60 C. Wu, Y. C. Wang, T. F. Lin, H. L. Tsao and P. C. Chen, Removal of arsenic from waste water using surface modified diatomite, *J. Chin. Inst. Environ. Eng.*, 2005, **15**, 255–261.

 This journal is © The Royal Society of Chemistry 2020